



Interinstrument calibration using magnetic field data from the flux-gate magnetometer (FGM) and electron drift instrument (EDI) onboard Cluster**

R. Nakamura¹, F. Plaschke¹, R. Teubenbacher^{1,*}, L. Giner², W. Baumjohann¹, W. Magnes¹, M. Steller¹, R. B. Torbert³, H. Vaith³, M. Chutter³, K.-H. Fornaçon⁴, K.-H. Glassmeier⁴, and C. Carr⁵

¹Space Research Institute, Austrian Academy of Sciences, 8042 Graz, Austria

²Graz University of Technology, 8010 Graz, Austria

³University of New Hampshire, Durham, NH 03824, USA

⁴Institut für Geophysik und extraterrestrische Physik, Technische Universität Braunschweig, 38106 Braunschweig, Germany

⁵Blackett Laboratory, Imperial College London, London, UK

* now at: Materials Center Leoben Forschung GmbH, Leoben, Austria

Correspondence to: R. Nakamura (rumi.nakamura@oeaw.ac.at)

Received: 31 May 2013 – Published in Geosci. Instrum. Method. Data Syst. Discuss.: 30 July 2013

Revised: 13 December 2013 – Accepted: 15 January 2014 – Published: 22 January 2014

** This paper is dedicated to the memory of Edita Georgescu.

Abstract. We compare the magnetic field data obtained from the flux-gate magnetometer (FGM) and the magnetic field data deduced from the gyration time of electrons measured by the electron drift instrument (EDI) onboard Cluster to determine the spin-axis offset of the FGM measurements. Data are used from orbits with their apogees in the magnetotail, when the magnetic field magnitude was between about 20 and 500 nT. Offset determination with the EDI–FGM comparison method is of particular interest for these orbits, because no data from solar wind are available in such orbits to apply the usual calibration methods using the Alfvén waves. In this paper, we examine the effects of the different measurement conditions, such as direction of the magnetic field relative to the spin plane and field magnitude in determining the FGM spin-axis offset, and also take into account the time-of-flight offset of the EDI measurements. It is shown that the method works best when the magnetic field magnitude is less than about 128 nT and when the magnetic field is aligned near the spin-axis direction. A remaining spin-axis offset of about 0.4 ~ 0.6 nT was observed for Cluster 1 between July and October 2003. Using multipoint multi-instrument measurements by Cluster we further demonstrate the importance of the accurate determination of the spin-axis offset when estimating the magnetic field gradient.

1 Introduction

Magnetic field and plasma environments of the Earth and other bodies in the solar system have been studied in situ since decades (Balogh, 2010). Therefore, magnetic field experiments onboard of spacecraft are of primary importance. Most commonly, flux-gate magnetometers (FGMs) are used due to their high accuracy, measurement range, resolution, and stability, paired with reasonable mass, power consumption, level of complexity, and overall costs (Acuña, 2002).

A FGM that is able to measure the strength and direction of the ambient magnetic field (\mathbf{B}) with high precision, requires extensive pre-flight (ground-based) and in-flight calibration (e.g., Glassmeier et al., 2007; Auster et al., 2008). The aim of the calibration is to determine 12 parameters needed to convert raw measurements (\mathbf{B}_{raw}) into components of a magnetic field vector (\mathbf{B}_{cal}) in a usable coordinate system (e.g., Kepko et al., 1996). The calibration parameters are six angles describing the orientation of the sensor axes in, e.g., a spacecraft-fixed frame of reference (constituting matrix \mathbf{M}), three gain values (elements of a diagonal matrix \mathbf{G}), and three zero level offset values (elements of vector \mathbf{O}). Therewith, the conversion of \mathbf{B}_{raw} into \mathbf{B}_{cal} is given by (e.g., Kepko et al., 1996; Acuña, 2002; Auster et al., 2008)

$$\mathbf{B}_{\text{cal}} = \mathbf{G} \cdot \mathbf{M} \cdot \mathbf{B}_{\text{raw}} - \mathbf{O}. \quad (1)$$

Despite pre-flight calibration under a variety of conditions (magnetic fields, temperatures), in-flight calibration remains necessary to account for slight changes of the calibration parameters during launch, instrument drifts over time while the mission proceeds, and, most importantly, spacecraft-caused disturbances which are beyond the scope of ground-based tests.

Variations in ambient magnetic field strengths and temperatures may have a minor influence on gain levels (\mathbf{G}) and orientations (\mathbf{M}) of the sensor axes relative to the spacecraft body. Spacecraft generated fields (e.g., due to electrical currents or magnetic materials) strongly contribute to the zero level offsets (\mathbf{O}), as these offsets represent the field values measured under the absence of an external magnetic field. Influence of the spacecraft on the magnetic field measurements can be reduced either by placing the FGM sensor on a long boom (e.g., Dougherty et al., 2004), hence, furthest possible away from the spacecraft's main structure, or by implementation of a magnetic cleanliness program (e.g., Ludlam et al., 2008). Unfortunately, both measures tend to be extremely expensive.

Spin stabilization of the spacecraft greatly supports the in-flight calibration process, as the presence and content of spin tone and/or higher harmonics in the magnitude and/or spin-axis component of \mathbf{B}_{cal} is influenced by 8 of the 12 calibration parameters (see, Auster et al., 2002), namely the spin-plane components of \mathbf{O} (which shall be O_1 and O_2), the ratio of the spin-plane components of \mathbf{G} (i.e., G_{11}/G_{22}), and five elements of \mathbf{M} (all but the angle defining the absolute orientation of the two spin-plane axes within that plane).

The in-flight determination of the spin-axis component of \mathbf{O} (which we denote with O_3) is often dependent on the availability of prolonged solar wind observations, where Alfvénic fluctuations are prevalent. These fluctuations are characterized by rotations in the magnetic field while the field strength ($|\mathbf{B}|$) remains constant. Hence, O_3 can be determined by minimization of variance of $|\mathbf{B}_{\text{cal}}|$ while observing Alfvénic fluctuations, as proposed in Hedgecock (1975). Improvements to his method are discussed in Leinweber et al. (2008) and, more recently, in Pudney et al. (2012).

If solar wind measurements are not available, O_3 may be determined with the help of complementary magnetic field observations, for instance from an electron drift instrument (EDI), which is the main subject of this paper. The EDI (Paschmann et al., 1997, 2001) onboard Cluster consists of two electron gun/detector units placed on opposite sides of the spacecraft, similar to that flown on the Equator-S spacecraft (Paschmann et al., 1999). Amplitude-modulated electron beams are fired by the two guns in specific directions. They perform one (or more) gyrations due to the ambient magnetic field and are eventually collected by the detectors after times T_1 and T_2 . The primary objective of the EDI is to measure the drift of the electrons caused by electric fields or magnetic field gradients.

The drift step, $\mathbf{d} = \mathbf{v}_d T_g$, during the gyration time T_g (drift velocity: \mathbf{v}_d) is a direct result from EDI measurements: small d can be determined by triangulation, based on the two beam-firing directions (for a detailed description see, Paschmann et al., 1997; Quinn et al., 1999). Large d are more accurately determined by time-of-flight observations of the two beams (Paschmann et al., 1997; Vaith et al., 1998). These times are different for electron release in parallel or anti-parallel directions to \mathbf{v}_d : $T_{1,2} = T_g(1 \pm |\mathbf{v}_d|/|\mathbf{v}_e|)$, where \mathbf{v}_e is the electron velocity dependent on their (known) kinetic energy: the sum of T_1 and T_2 yields twice the gyration time T_g , their difference is proportional to d (Paschmann et al., 1999). The use of different electron energies further allows one to distinguish drifts caused by electric fields or magnetic field gradients (see, Paschmann et al., 1997).

Since the gyration time T_g is inversely proportional to the magnetic field strength $|\mathbf{B}|$, EDI measurements allow for a determination of ambient $|\mathbf{B}|$:

$$|\mathbf{B}| = \frac{2\pi m_e}{e T_g}, \quad (2)$$

where m_e is the electron mass and e the elementary charge. These values are practically not influenced by spacecraft fields, as electrons perform most of their gyration at sufficient distances from the spacecraft. Hence, they are ideally suited as a reference for FGM measurements. Comparison of EDI and FGM magnetic field data yields FGM zero level offset vectors \mathbf{O} and, in particular, their spin-axis components O_3 , as shown by Georgescu et al. (2006).

Their methods were developed further by Leinweber et al. (2012) in order to obtain absolute spin-plane and spin-axis FGM gains (i.e., G_{11} and G_{22} with constant ratio G_{11}/G_{22} , and G_{33}), in addition to O_3 , with the help of EDI time-of-flight $|\mathbf{B}|$ values. Note that the spacecraft spin does not support calibration of any of these three parameters, as they do not influence the content of spin tone or higher harmonics in \mathbf{B}_{cal} .

Both studies (Georgescu et al., 2006; Leinweber et al., 2012), however, do not take into account that the time-of-flight measurements themselves are known to be subject to offsets (Georgescu et al., 2012). T_1 and T_2 values differ systematically from the respective true values; and deviations depend on instrument mode as we will show later.

Accurate calibration of FGM gains and zero level offsets with EDI $|\mathbf{B}|$ measurements is only possible if electron time-of-flight offsets are previously determined and corrected for. In this paper, we show how this can be achieved by using Cluster data from the EDI and FGM (Balogh et al., 2001) and present the possible schemes of interinstrument calibration. We further examine the characteristics of the FGM spin-axis offsets in the low field region and demonstrate the importance of accurate calibration when determining magnetic field gradient using multipoint Cluster measurements.

2 Method of analysis: interinstrument calibration

Since our main interest is to determine the spin-axis offset component, we use the flux-gate spin reference (FSR) coordinates, where Z points along the spin axis and X and Y are the spin-plane components. Here we assume that except for some residual spin-axis offset, $\Delta B_{Z_{\text{fgm}}}$, all the calibration parameters have been accurately determined. Since the time-of-flight data provide the magnitude of the magnetic field, B_{edi} , from Eq. (2) we use the spin-plane components of the FGM data to deduce the spin-axis component, $B_{Z_{\text{edi}}}$:

$$B_{Z_{\text{edi}}}^2 = B_{\text{edi}}^2 - B_{X_{\text{fgm}}}^2 - B_{Y_{\text{fgm}}}^2. \quad (3)$$

The spin-axis offset, $\Delta B_{Z_{\text{fgm}}}$, can then be obtained from

$$|B_{Z_{\text{edi}}}| = |B_{Z_{\text{fgm}}} + \Delta B_{Z_{\text{fgm}}}|, \quad (4)$$

if the spin-axis component of the magnetic field deduced from the EDI time-of-flight measurements and the spin-plane component of the FGM magnetic field are obtained with sufficient quality.

For determining B_{edi} , we have simply used all the time-of-flight data from the two gun-detector units, GDU1 and GDU2, without identifying the pairs of long and short time of flight to obtain the gyration time from their average, such as described before, based on an assumption that the usage of large numbers of data of both times of flight is equivalent to effectively averaging the measurement pairs. We use the high resolution FGM data (22.4 Hz for normal mode) and match them with the nearest neighbor to the EDI time-of-flight data. The EDI time-of-flight data are irregularly spaced data with a smallest interval of 16 ms, but are sparse compared to the FGM data, since detection of the returning electron beam is required.

In this study we use Cluster data from July to October 2003 and from July to October 2006, when the apogee of Cluster orbit is at night side. The interspacecraft distance was on the order of 200 km in 2003 and 10 000 km in 2006. During these summer seasons, when Cluster stayed in the magnetosphere and no solar-wind data were available, it is of particular interest to determine the FGM offset using the EDI measurements since the Hedgecock method (Hedgecock, 1975) cannot be applied. Furthermore, one of the scientific interests in the tail region is the magnetic reconnection process, for which the magnetic field component normal to the current sheet, corresponding to the spin-axis component, is key in detecting the process. Hence an accurate determination of the spin-axis component is crucial in this region.

Since both the FGM and EDI instruments are designed to obtain optimized field measurements in different regions of space, the digital resolution of the measurements change. In this study we analyzed magnetic field data with magnitudes less than 600 nT. For FGM, within our region of interest, this corresponds to 3 different ranges, i.e., digital resolutions, changing from 7.813 to 0.125 nT depending on the

field magnitude as will be discussed later. The EDI time-of-flight measurement, however, is operated by tracking electron beams that are amplitude-modulated with a pseudonoise (PN) code, with a certain code period, T_{PN} , or alternatively represented as the code repetition frequency (CRF), which is $1/T_{\text{PN}}$. The PN code consists of either a 15-chip or 127-chip code with different code chip lengths, T_{chip} . The accuracy of EDI measurements depend on the T_{chip} , and therefore T_{PN} or CRF, which is usually given in unit of kilohertz. T_{PN} varies between 30 μs and 2 ms for the data set used in this study. The time resolution of EDI is defined by the shift-clock period, which is the shift in the PN code to track small time-of-flight variations, that varies from 1.907 to 0.119 μs depending on the magnetic field; see more details in Georgescu et al. (2006). Further details about these parameters and the EDI operation schemes are given by Vaith et al. (1998) and Paschmann et al. (2001). Here we call the different measurement settings of the EDI “CRF mode” for convenience. As will be discussed later in more detail, these different resolutions/modes need to be taken into account when data are calibrated.

Figure 1 shows FGM and EDI magnetic field magnitude data during a quiet interval of about 3 min from Cluster 3 for different FGM calibration schemes. The FGM data shown in the three left panels a–c use the orbit calibration file provided for the Cluster Active Archive (CAA) data set (Gloag et al., 2006), the three middle panels d–e use the daily calibration file (Fornaçon et al., 2011) used for the Cluster Prime Parameter (PP) and Summary Parameter (SP) data set in the Cluster Science Data System (CSDS), and the three right panels g–i use the fine-tuned calibration file using the daily calibration file as an input. Figure 1a shows the magnetic field magnitude data estimated from EDI and FGM, in which the latter data are time-matched data to EDI using the nearest neighbor data selected from the high-time resolution (22.4 Hz) data shown in Fig. 1b. Although the example shown here is from a period when the numbers of the returning beams are quite evenly distributed all the time, EDI data depend on the availability of the returning beam and can be also sparse in time. Hence it is essential to compare EDI data with the time-matched FGM data. Figure 1c shows 1 Hz averaged data for both FGM and EDI. It can be seen that both data sets have a small standard deviation (about 0.1 nT) during this interval and there exists a clear difference between FGM and EDI magnitudes of about 0.5 nT. The same comparison has been done for data calibrated using the daily calibration file (Fig. 1d–f). The 22.4 Hz data have a slightly larger standard deviation compared to the CAA data, but the difference between EDI and FGM is smaller, about 0.14 nT. The relatively large scatter of the 1 Hz data (Fig. 1f) comes from the spin-tone, which can be more clearly seen in the 22 Hz data (Fig. 1e). Data shown in Fig. 1g–i are using the same daily calibration file, as was used for data in Fig. 1d–f, as input and then further refined the calibration file to reduce the spin tone. This additional procedure, however, has little effect on the average

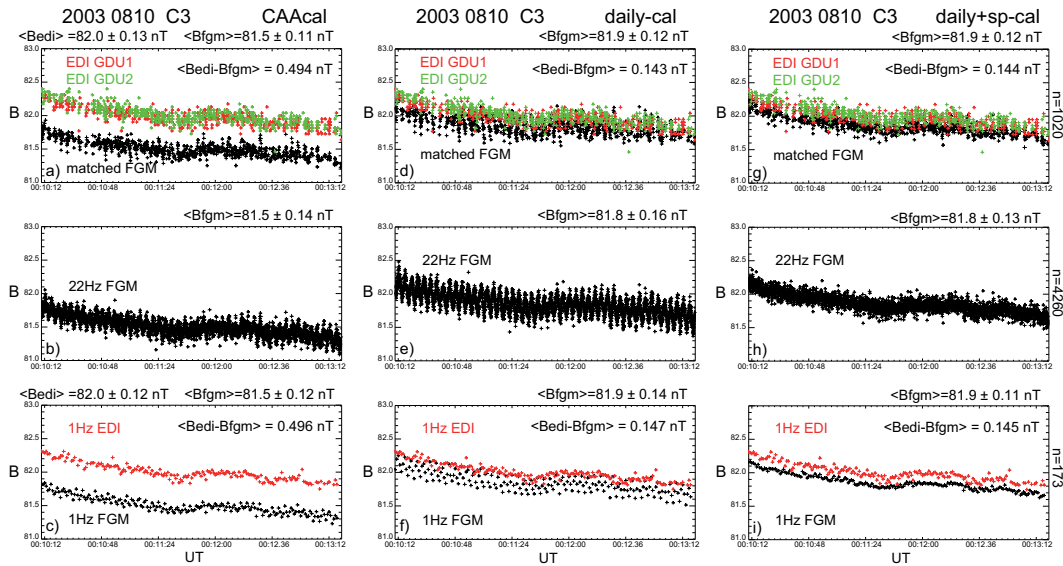


Fig. 1. FGM and EDI magnetic field magnitude data during a quiet interval from Cluster 3 using FGM data with different calibration schemes: the orbit calibration, method used for CAA data set (a–c); daily calibration method used for CSDS data set (d–f); and refined calibration applied to daily calibration input (g–i). The upper three panels (a, d, g) show high-resolution EDI and time-matched FGM 22.4 Hz data, the middle three panels (b, e, h) show the 22.4 Hz FGM data, and the lower three panels (c, f, i) show 1 Hz averaged data for both FGM and EDI.

FGM–EDI difference as can be seen in the numbers obtained for the high-resolution data (Fig. 1d, g) and for the 1 Hz data (Fig. 1f, i). Note that for following discussions on offset calibration procedure we use the daily calibration file, prepared since the Cluster launch by the Technical University of Braunschweig Cluster Co-I team. That is, we use the same data set as shown in Fig. 1d–f. It should be therefore noted that when we write “spin-axis offset” in this paper, we are not speaking about an offset from the raw data as given in the Eq. (1), but about a remaining offset correction from an already in-flight calibrated data set.

Figure 2a shows the number of EDI time-of-flight data points from Cluster 1 in August 2003, when corresponding FGM data were available, binned by the magnitude of the field, B_{fgm} . The size of the bins is 16 nT. The number of points are grouped by different CRF modes. Note that these different CRF modes generally correspond to data from different field magnitude regions, which are marked as R1–R6 next to the legend. More details of the meaning of these different magnitude regions, R1–R6, and the EDI measurement resolution are explained later (Fig. 3). It can be seen in the histogram that for smaller field regions, in particular, the EDI observations have been made with several different CRF modes. Figure 2b shows the differences between the $|B_{Z_{\text{edi}}}|$ and $|B_{Z_{\text{fgm}}}|$. The bin averages (dotted line) and medians (solid line) are also depicted in the figure. When both B_Z values are positive, it corresponds to the spin-axis offset. It can be seen that the values are widely scattered, particularly with increasing magnitude of the field. Also, instead of seeing a constant offset value of FGM, the difference is increas-

ing with magnetic field magnitude but not monotonically. As will be discussed below, these variable differences can be due to (i) the effects of different magnetic field angles relative to the spin axis, (ii) the different CRF modes of the instruments and different offsets, and (iii) the effects from variable calibration parameters other than the offsets considered here. In the following we mainly examine the first two effects when obtaining the spin-axis offset of FGM and further discuss the possible effect due to (iii) based on the obtained offsets.

Since we are interested in the spin-axis offset, it is important to use measurements with sufficient magnitude of the spin-axis direction. As mentioned before, a meaningful comparison of the two spin-axis components using Eq. (4) can only be performed when both have the same (positive, for majority of the data used in this study) sign even when the possible offset values are subtracted, because Eq. (3) does not provide the sign of the magnetic field along the spin axis. The unknown sign of the $B_{Z_{\text{edi}}}$ will lead to miscalculation when the spin-axis offset effect changes the sign of the spin-axis component. This corresponds to cases when the expected spin-axis offset becomes significant compared to the spin-axis component of the magnetic field. Considering that we use an already calibrated data set as an input, a typical offset value is expected to be small, i.e., less than a couple of nanoteslas. For the Cluster data we are examining in this paper, such offset can be more than 10 % of the field magnitude. Hence we need to take into account only data when $|\cos b| \equiv |B_{Z_{\text{fgm}}}/B_{\text{fgm}}|$ is sufficiently large so that the offset subtraction will not make any difference in the change

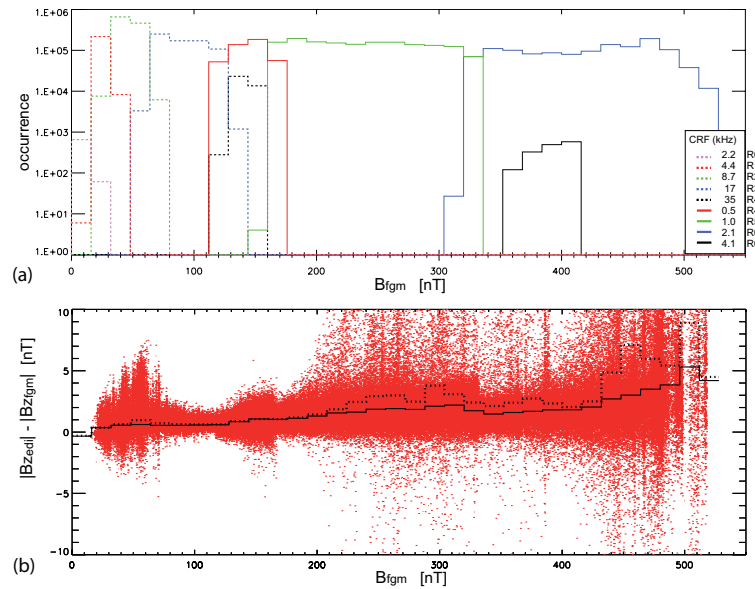


Fig. 2. (a) Number of points for all available Cluster 1 EDI data in August 2003, binned by the magnitude of the field B_{fgm} . The size of the bins is 16 nT. The number of points are grouped for different CRF modes (see details in text). (b) Differences between $|B_{Z_{edi}}|$ and $|B_{Z_{fgm}}|$ for the same data set. The solid line shows the median and the dotted line shows the average of the data within each bin. Here every 20th point from the entire data set shown in (a) is plotted.

of sign. As we will show later, $|\cos b| \geq 0.4$ would typically work for the analysis.

In this study we consider a time-of-flight offset of EDI, ΔT_{edi} , which is expected to have different values for different CRF modes. For simplicity we assume the same offset value for the time-of-flight measurements from GDU1 and GDU2. That is, when calculating the magnetic field from EDI measurement, we use

$$B_{edi} = \frac{2\pi m_e}{e(T_{edi} + \Delta T_{edi})}, \quad (5)$$

to determine both ΔT_{edi} and $\Delta B_{Z_{fgm}}$ from the data, instead of Eq. (2).

Significance of the EDI and FGM offsets varies for different field magnitudes as is shown in Fig. 3. The four solid curves in Fig. 3a show the effective spin-axis offset value caused by an EDI time-of-flight offset, $\Delta T_{edi} = 0.5 \mu s$, that will appear when the EDI and FGM measurements are compared, such as in Fig. 2. They are plotted for different angles of the magnetic field, $\cos b$. Here, the effective EDI magnetic field measurement resolution based on the digital resolution of the EDI measurements discussed by Georgescu et al. (2006) is also given as a dashed curve for the different magnetic field regions, R1–R6, as indicated at the bottom of Fig. 3b. The borders of R0–R6 are shown with the vertical dotted line, which corresponds to 16, 32, 64, 128, 164, and 326 nT. The horizontal brown line indicates the 0.5 nT level, as a typical number for the spin-axis offset of FGM. In a similar way, we plotted the effective time-of-flight offsets caused by a FGM spin-axis offset of $\Delta B_{Z_{fgm}} = 0.5$ nT. The

dashed lines indicate the same EDI digital resolution of the time-of-flight measurement as given in Fig. 3a. The horizontal brown line shows 0.5 μs as a typical number for the time-of-flight offset of EDI. It can be immediately seen that the time-of-flight offset will have no effect in the small field region regardless of the angle to the magnetic field (brown line located above the curves in Fig. 3). Therefore, these curves show that the different angle of the fields as well as the time-of-flight offset can easily cause the large scatter of points in Fig. 2b. One can also conclude that for determining the offset in B_Z in a given field magnitude, it would be most effective to use data from large $\cos b$, since the relative importance of the EDI time-of-flight offset would be smallest. Furthermore, in the low-field region, a time-of-flight offset of about 0.5 μs will have only negligible effect in the spin-axis component of the magnetic field, which is a value below the instrument resolution. In the high-field region, however, a 0.5 nT spin-axis offset is a negligible value in the time-of-flight data and comparable to the resolution of the EDI measurement. It is also important to note that when we determine ΔT_{edi} , it is most efficient to use data with low $\cos b$, i.e., when the field direction is mainly along the spin-plane direction. Vice versa, $\Delta B_{Z_{fgm}}$ should be determined for large $\cos b$ as mentioned before. Due to these variable effects over the field magnitude, we need to consider different approaches for different magnetic field magnitudes depending on the importance of the offset. In Sect. 3 we demonstrate an example of a calibration in which all the different offsets are obtained using a large number of points and for different magnetic field magnitude

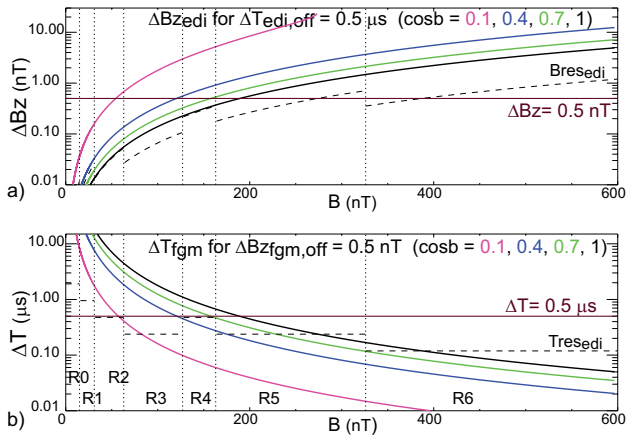


Fig. 3. (a) The effective spin-axis offset value caused by an EDI time-of-flight offset, $\Delta T_{\text{edi}} = 0.5 \mu\text{s}$, that will appear when the EDI and FGM measurements are compared, plotted for selected angles of the magnetic field, $\cos b$. The dashed lines show the resolution of the EDI magnetic field measurement. The horizontal brown line shows 0.5 nT level, which represents a typical number for the spin-axis offset of FGM. (b) The effective time-of-flight offsets caused by a FGM spin-axis offset, $\Delta B_{Z\text{fgm}} = 0.5 \text{ nT}$, plotted for selected values of $\cos b$. The dashed lines indicate the EDI digital resolution of the time-of-flight measurement. The horizontal brown line shows the 0.5 μs level, which represents a typical number for the time-of-flight offset of EDI. The vertical dotted lines indicate the border of different EDI measurement settings, R0–R6. See text for further details.

regions. We also specifically use data from the low-field region to examine the possibility for estimating an offset with a small number of samples.

3 Example of interinstrument calibration

Figure 4a shows the number of EDI measurements from Cluster 1 in August 2003 in the same format as in Fig. 2a, but only for $\cos b > 0.7$. As discussed before, this condition angle allows one to select data when the relative importance of the B_Z offset is higher than the possible time-of-flight offset, and additionally to fulfill the condition of the same positive sign of FGM and EDI in spin-axis components. As discussed before, EDI is operated with different CRF modes in different magnetic field regions. For this field angle, data were available only between the regions R2 and R6 (see Fig. 3 for definition of the regions). The FGM range changes at 256 nT, which is a value within R5. Depending on the importance of the offset, we determined ΔT_{edi} or $\Delta B_{Z\text{fgm}}$ in the following way.

- Low-field region (R1–R3), when the effect of $\Delta B_{Z\text{fgm}}$ is important: $\Delta B_{Z\text{fgm}}$ is first determined for $\cos b > 0.7$. ΔT_{edi} is then determined using data obtained for R1–R3 separately.

- Mid-field region (R4), when both effects from EDI time of offset and FGM offset in spin-axis component are comparable: ΔT_{edi} is determined using $\Delta B_{Z\text{fgm}}$ determined for R2–R3. Since there are two different CRF modes used for EDI measurements in this region, we calculated the time-of-flight offsets for each CRF mode separately.

- Mid-field region (R5), when both effects are comparable and FGM range changes within the same EDI CRF mode: same method as R4 is used for data with $B_{\text{fgm}} < 256 \text{ nT}$. Determine $\Delta B_{Z\text{fgm}}$ for $\cos b > 0.7$ using ΔT_{edi} determined for R5 data with $B_{\text{fgm}} < 256 \text{ nT}$.

- High-field region (R6), when the effect of ΔT_{edi} is important: determine ΔT_{edi} taking into account the FGM offset determined for R5. Since the effect of spin-axis offset is not important regardless of $\cos b$ all data are used.

Figure 4b shows the FGM and EDI differences of original calibrated data as shown in Fig. 2 except for $\cos b > 0.7$. The bin averages and median are shown as solid lines, although the difference between the two are hardly recognizable in this plot.

The average profile in Fig. 4b shows some jumps coinciding with CRF-mode change and more monotonic increase in the high-field region within the same CRF mode as expected in the curve shown in Fig. 3a. Figure 4c shows the results of the calibration procedure for August 2003. The points are the differences between the offset-corrected FGM and EDI data. The lines again show the bin average and the median of the differences of the offset-corrected FGM and EDI data. Here again the differences between the two lines are hardly seen. It can be seen that the bin average (or median) runs at almost the zero level except for some fluctuations of $\leq 0.1 \text{ nT}$ in the higher field region. The nearly zero level of the bin's average (or median) profile suggests that the spin-axis component difference between EDI and FGM was well explained due to the spin-axis offset of FGM and time-of-flight offset of EDI.

Table 1 provides the monthly average results of the different offsets between July and October 2003 for Cluster 1: $\Delta B_{Z\text{fgm}}$ for low field range ($< 256 \text{ nT}$) and high field range ($> 256 \text{ nT}$) and ΔT_{edi} for different CRF modes, corresponding to R1–R6 (as given in the legend in Fig. 4a). Although we used all the available data without selecting, for example, quiet time data, it can be seen that $\Delta B_{Z\text{fgm}}$ determined from the low field region (R2–R3), which corresponds to $B \sim 32\text{--}128 \text{ nT}$, stays at about 0.4–0.6 nT with a relatively small standard deviation. The standard deviation is quite large for the FGM offset at the high-field region (R5), while the values stay at a similar value to the low-field region within 0.1 nT during the four months. ΔT_{edi} , however, is stably obtained only in the field region larger than about 128 nT (R4–R6), while the time-of-flight offsets could be poorly

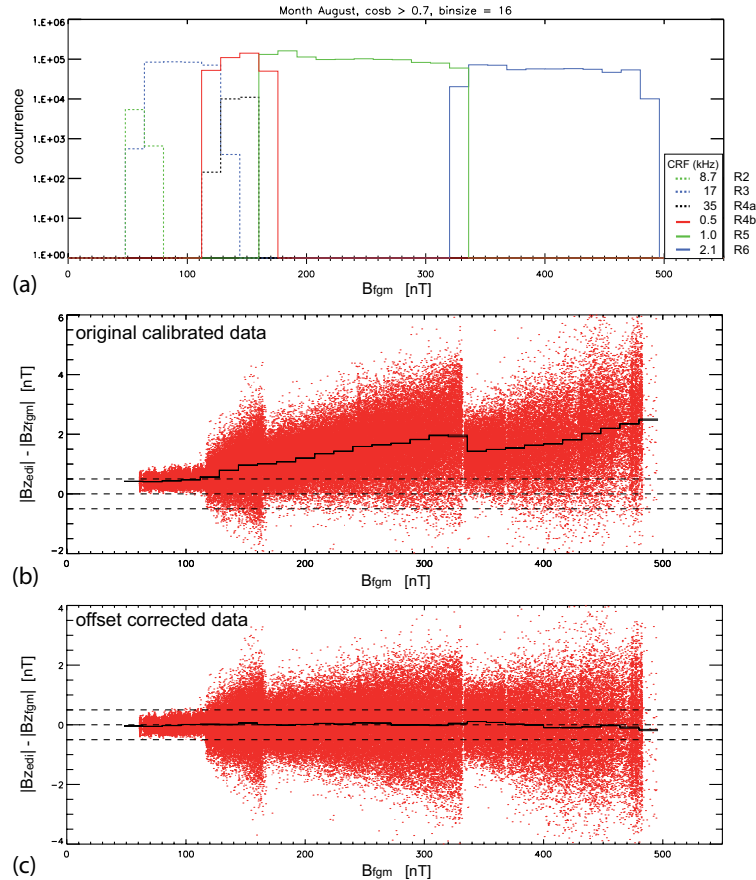


Fig. 4. (a) Number of points for Cluster 1 EDI data in August 2003 binned by the magnitude of the field B_{fgm} as in Fig. 2 except for $\cos b > 0.7$. Difference between spin-axis component EDI and FGM fields for $\cos b > 0.7$ (b) for the original calibrated data and (c) for the offset-corrected data. Bin average and median for the original and offset-corrected data are shown in each panel. Note that both curves are nearly identical and therefore their differences can hardly be seen. As in Fig. 2, every 20th point from the corresponding data sets given in panel (a) is plotted. Dashed lines indicate -0.5 , 0.0 , and 0.5 nT levels.

determined with a large standard deviation only in the low-field region. This behavior can be understood with the characteristics of resolution of the EDI measurements (Fig. 3), i.e., finer B resolution of EDI for the smaller field region, and smaller (larger) effect of ΔT_{edi} in a smaller (larger) field region relative to the effect of $\Delta B_{Z\text{fgm}}$. Except for the poorly determined ΔT_{edi} (R1–R3), the values shown in Table 1 were used to calculate the points in Fig. 4c.

We have performed the same procedure for every orbit in August 2003 for Cluster 1 and the results are shown in Fig. 5. $\Delta B_{Z\text{fgm}}$ for the low field (< 256 nT) and high field (> 256 nT) and their corresponding numbers of points are shown in Fig. 5a and b, respectively. As described before, low-field data points are from EDI CRF modes for R2 and R3 (see Fig. 4b), while high-field data points are from EDI CRF modes for R5. ΔT_{edi} for each orbit in R2, R5, and R6 and the corresponding numbers of data points are shown in Fig. 5c and d. Note that measurements in low field regions did not take place in every orbit in this month and therefore

Table 1. Average offsets determined for different modes/ranges for Cluster 1.

| Parameters | July 2003 | August 2003 | September 2003 | October 2003 |
|-----------------------------------------------|-----------------|-----------------|-------------------|-----------------|
| $\Delta B_{Z\text{fgm},1}$ [nT] | 0.51 ± 0.15 | 0.46 ± 0.16 | 0.64 ± 0.17 | 0.57 ± 0.17 |
| $\Delta B_{Z\text{fgm},h}$ [nT] | 0.40 ± 0.99 | 0.41 ± 0.99 | 0.57 ± 1.04 | 1.00 ± 0.19 |
| $\Delta T_{\text{edi},R1}$ [μs] | 2.92 ± 5.77 | 1.90 ± 4.77 | 2.87 ± 6.42 | 1.92 ± 4.98 |
| $\Delta T_{\text{edi},R2}$ [μs] | 1.81 ± 2.42 | 1.60 ± 1.96 | 1.81 ± 1.89 | 1.85 ± 2.40 |
| $\Delta T_{\text{edi},R3}$ [μs] | 0.38 ± 1.15 | 1.03 ± 1.27 | 0.70 ± 0.89 | 1.20 ± 1.04 |
| $\Delta T_{\text{edi},R4a}$ [μs] | 0.21 ± 0.25 | 0.15 ± 0.20 | 0.19 ± 0.16 | 0.05 ± 0.23 |
| $\Delta T_{\text{edi},R4b}$ [μs] | 0.65 ± 0.97 | 0.63 ± 0.96 | 0.50 ± 0.97 | 0.48 ± 1.00 |
| $\Delta T_{\text{edi},R5}$ [μs] | 0.55 ± 0.42 | 0.55 ± 0.43 | 0.59 ± 0.46 | 0.57 ± 0.50 |
| $\Delta T_{\text{edi},R6}$ [μs] | 0.28 ± 0.19 | 0.26 ± 0.19 | 0.27 ± 0.19 | 0.26 ± 0.20 |

values using those data points can only be seen every second or fourth orbit. It can be seen that $\Delta B_{Z\text{fgm}}$ obtained from the low-field region is relatively stable compared to that obtained from the high-field region. As for ΔT_{edi} , the values of R6 are most stable among the three offsets. ΔT_{edi} is larger for R2

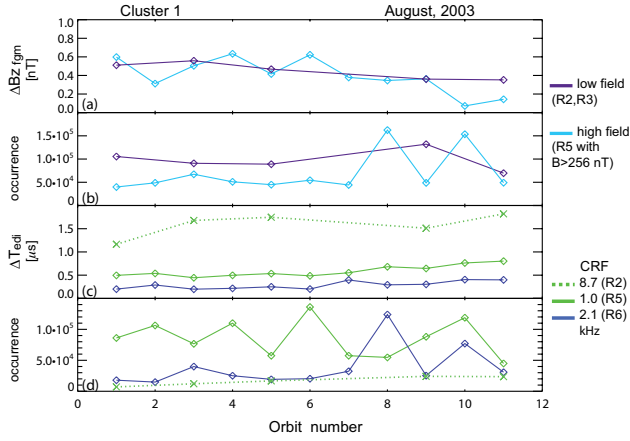


Fig. 5. (a) ΔB_{Zfgm} determined for every orbit in the low field (< 256 nT) and high field (> 256 nT) and (b) the corresponding numbers of data points from Cluster 1 in August 2003. (c) ΔT_{edi} for each orbit in R2, R5, and R6 and (d) corresponding numbers of data points.

compared to R5 and R6; yet the effect from ΔB_{Zfgm} can still be expected to dominate in R2 for these values (see Fig. 3).

The spin-axis direction, which is approximately the Z direction in geocentric solar ecliptic (GSE) coordinates, is closely aligned to the normal component of the current sheet in the magnetotail, where the apogee is located for Cluster between July and October. This normal component drops to zero when magnetic reconnection occurs, which is an important science target in magnetospheric missions such as Cluster as well as for the upcoming Magnetospheric Multiscale (MMS) mission. Therefore, to detect the process accurately, it is required that the spin-axis offset be corrected. It is therefore desirable that the calibration will take place close to such target intervals, that is, in a relatively small field region when the disturbance of the field is small. Below we use Cluster data for a short interval, i.e., several minutes, in a small field region, such as the example shown in Fig. 1, to examine the effect of the spin-axis component offset in the difference between FGM and EDI magnetic fields. We searched for quiet and constant field intervals using data between July and October 2003 in small field region (R2), corresponding to the magnetic field between about 30 and 60 nT. A quiet field's short time interval is defined as an interval with standard deviation less than 0.1 nT. We chose a time period of 7 min. We obtained 579 such intervals for C1 during the four months. Figure 6a and b show the magnitude difference, $\Delta B \equiv B_{edi} - B_{fgm}$, and difference in the spin-axis components, $\Delta B_Z \equiv |B_{Zedi}| - |B_{Zfgm}|$, plotted vs. the field angle, $\cos b$. On average, the magnitude difference is small when the magnetic field is nearly aligned to the spin plane (small $|\cos b|$) within an error of about 0.1 nT and justifies our assumption that the main discrepancy between the two data sets are attributed to the spin-axis offset. When the

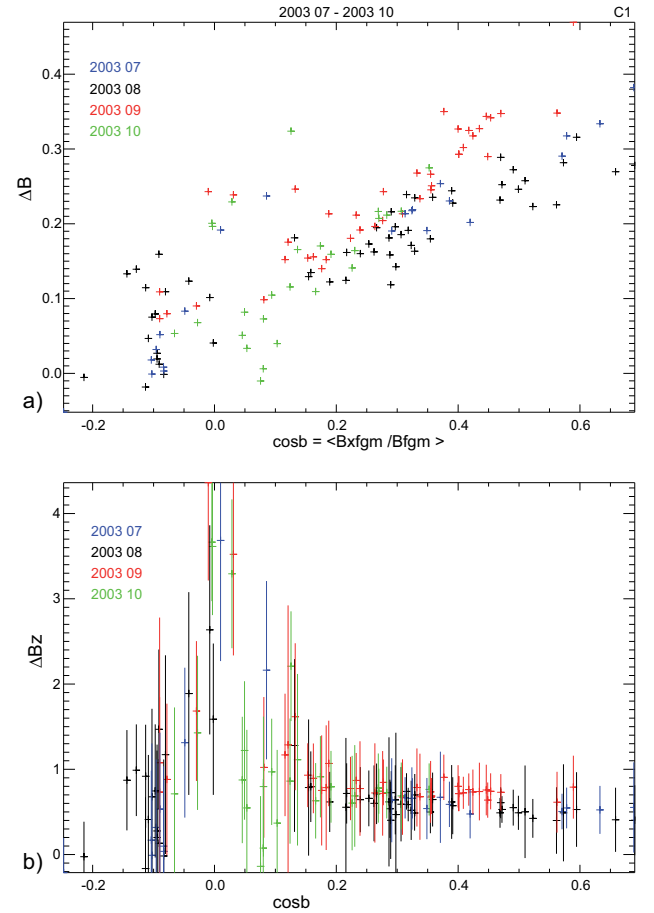


Fig. 6. (a) Average magnitude difference, $\Delta B \equiv B_{edi} - B_{fgm}$, and (b) average difference in the spin-axis components, $\Delta B_Z \equiv |B_{Zedi}| - |B_{Zfgm}|$, plotted vs. the field angle, $\cos b$, obtained using quiet, low field (30–60 nT), short time interval (7 min) data sets in July–October 2003. The vertical bars in (b) show the standard deviation.

$|\cos b|$ is small, $|\cos b| < 0.1$, it is not possible to obtain the correct sign of ΔB_Z . In such cases the comparison between the spin-axis components will contain large errors. That is, we may obtain the sums of the two measurements instead of differences, meaning that the ΔB_Z will rather become twice the average of the spin-axis component value ($2B \cos b$). If we assume, for example, that such errors happen in about half of the cases we can expect an average to be estimated as $B \cos b$. For the field magnitude in this data set, i.e., $B = 30$ – 60 nT, a “wrongly” estimated ΔB_Z of ≤ 3 – 6 nT can be expected for $\cos b \leq 0.1$, which was in fact the case as shown in Fig. 6b. However, the spin-axis offsets are more stable for a larger $\cos b$, i.e., $\cos b \geq 0.4$, indicating the importance of preselection of the angle of the field when determining the spin-axis offset.

The essential advantage of multipoint measurements such as with Cluster is the ability to determine spatial gradients. We finally examine the possible effect of the offset

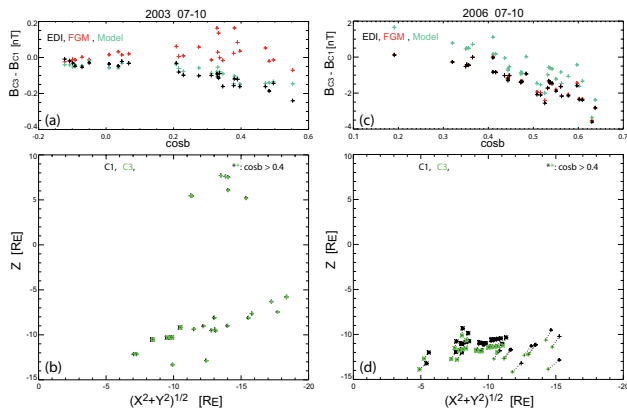


Fig. 7. Average magnetic field differences between C1 and C3 for B_{edi} (black cross) and B_{fgm} (red cross), and a model magnetic field (green cross) during quiet time intervals (standard deviation of $B_{\text{edi}} < 0.07$ nT for 5 min interval) plotted vs. $\cos b$ for data from (a) July to October in 2003, when the interspacecraft distance was about 200 km, and from (c) July to October in 2006, when the interspacecraft distance was about 10 000 km. The location of the spacecraft in GSM (geocentric solar magnetospheric) coordinates during these two sets of intervals are shown in (b) and (d), respectively.

calibration by comparing the magnetic field gradients (differences between two spacecraft) for B_{edi} , B_{fgm} , and an empirical magnetic field, i.e., combined IGRF and Tsyganenko 89, $K_p = 2$, as shown in Fig. 7. Here we select again quiet time intervals, when standard deviation of $B_{\text{edi}} < 0.07$ nT for 5 min intervals and when data from both Cluster 1 and 3 are available. Cluster data are used from an interval between July and October in 2003, when the interspacecraft distance was about 200 km, and between July and October in 2006, when the interspacecraft distance was about 10 000 km. Figure 7a shows the spacecraft differences, $\Delta B_{\text{edi},C1-C3}$ (black), $\Delta B_{\text{fgm},C1-C3}$ (red), and model (green), plotted again over $\cos b$ (of Cluster 1) observed at locations shown in Fig. 7c for the events in 2003.

The model provides a reference value of the magnetic field profile and is constructed based on fitting a number of previous satellite data. Therefore we can expect that the model represents some averages of different randomly distributed “offsets” among the different previous measurements providing an empirical value of the field. The $\Delta B_{\text{edi},C1-C3}$ and model generally agree well. This suggests that $\Delta B_{\text{edi},C1-C3}$ provides closer values to an empirical value of the magnetic field. $\Delta B_{\text{fgm},C1-C3}$ shows a smaller difference in the small $\cos b$ region, which corresponds to the magnetic field direction where the spin-axis component does not play a role, suggesting that the spin-plane components are well calibrated. The differences, however, become larger for larger $\cos b$ indicating that the effect of the spin-axis offset is apparent and causing these larger differences. Figure 7b and d show the results of the same analysis performed for the data in 2006 for comparison. In contrast to 2003, the gradients obtained from

the two measurements show similar values, while the model values deviate from these two. The interspacecraft distance of 200 km is small enough that the effect of the offset calibration exceeds the magnetic field gradient, while such offset determination plays no difference for the interspacecraft distance of 10 000 km. Hence, depending on the interest of the gradient scales it will become essential to perform special offset calibrations when determining the gradient of the magnetic field.

4 Discussion

Based on a simple comparison between the magnetic field of FGM and the magnetic field deduced from the time of flight of the EDI measurements, we have shown that the remaining spin-axis offset of FGM data can be well determined from the calibrated data set by selecting the appropriate interval, by taking into account the measurement conditions such as the angle of the magnetic field relative to the spin-plane, magnetic field magnitude, and by also considering the effect of the time-of-flight offset of the EDI measurement. While the effect of the time-of-flight offset was unimportant in determining the spin-axis offset in the low field region, it was the major source of the discrepancy between the two data sets in the large field region. Once the effects of these two offsets are taken into account, the difference between the two measurements are reduced to be well below the 0.1 nT level. Note that there is a tendency of somewhat larger fluctuations superposed with a negative trend for the larger field region (R6) in Fig. 4. This might suggest that some additional FGM gain correction needs to be considered. The current offset correction does not take into account any gain correction. If there is a gain error, it should appear as a linear trend if all the other calibration parameters are perfectly determined. Such gain error curve, however, is difficult to differentiate from the EDI time-of-flight profile particularly for a low-resolution measurement. Therefore each EDI range may show a different resultant curve and may not appear a continuous line in Fig. 4c even if there is a gain error. In the low field region, we cannot see any systematic trend, for example. If we take the ~ -0.1 nT deviation in the R6 region (covering an about 200 nT-wide region), as an observed number, it will correspond to a linear gain correction of 0.0005. Such change in the gain may likely happen due to the change in the temperature. Indeed if we use the ground-calibration result from one of the Cluster ground sensors, i.e., 0.00004 K^{-1} (Othmer et al., 2000), this corresponds to a gain drift for a temperature change of about 12° , which would not be an unrealistic variation within an orbit. For an accurate determination of the gain from these comparisons, however, only a statistical approach is possible because in this high-field region. EDI can measure the field only at a resolution of about 1 nT, while the effects expected from gain errors would be less than at a

0.1 nT scale, which is also below the FGM resolution in this range and therefore fluctuations are unavoidable.

While we demonstrate that the simple comparison is overall working, particularly for the spin-axis determination in low field regions, once we are interested to determine also other parameters, such as time-of-flight offsets throughout the EDI CRF modes or FGM offsets and gain factors for high field ranges, further investigations would be necessary. For example, our simplified approach of pre-selecting the data set based on specific conditions in angle and magnitude of the field, as discussed in Sect. 3, limits the number of useful data. Instead one may consider to use all the data from different field magnitudes (and therefore with different EDI CRF modes) and try to determine the EDI and FGM offsets at once by applying appropriate weighting factors that depend on the contribution of the EDI and FGM offsets in the measurement, and by minimizing the differences between the two measurements. Furthermore determining the EDI time-of-flight offset for the two GDUs, separately, may be also important particularly for mid- and high-field regions.

In this study we only used the time-of-flight data of the EDI measurements to compare with the FGM measurements. Another useful approach is to use the direction of the EDI electron beam, \mathbf{u}_{edi} , which should be perpendicular to the ambient magnetic field, and use the condition of $\mathbf{u}_{\text{edi}} \cdot (\mathbf{B}_{\text{fgm}} + \mathbf{O}_{\text{fgm}}) = 0$, to determine the offset of the FGM measurement, \mathbf{O}_{fgm} . A combination of these two methods will further improve the accuracy of the offset determination.

5 Conclusions

We have shown that the concept of determining the spin-axis offset of a flux-gate magnetometer (FGM) using absolute field magnitude data determined from the electron gyration time data of the electron drift instrument (EDI) works best when the magnetic field magnitude is small; i.e., less than about 128 nT corresponding to the EDI modes for the low field, so that the EDI time-of-flight offset is negligible, and when the spin-axis component becomes the major component ($\cos b > 0.7$). A remaining spin-axis offset of about 0.4 ~ 0.6 nT was observed for Cluster 1 between July and October 2003, which is important for studies using the magnetic field component normal to the current sheet in the central plasma sheet such as magnetotail reconnection or thin-current sheet dynamics or particle trajectories near the center of the current sheet.

When the effect of time-of-flight offset from EDI is taken into account, it is shown that data from higher fields can be also used for calibration. It is shown that additional determination of the gain factor of the FGM instrument would most likely also be possible.

The EDI–FGM comparison method is of particular interest for the observations, when no solar-wind data are available for calibration. It will play an essential role for accu-

rate determination of the small normal component (and its reversals) in the current sheet required for studying magnetic reconnection, which is the main objective of NASA's Magnetospheric Multiscale (MMS) mission.

Acknowledgements. This paper is dedicated to the memory of E. Georgescu, Max Planck Institute for Solar System Research, Germany. E. Georgescu initially started the EDI–FGM comparison work. Without her inspiring comments and suggestions this study would not have been done. We thank P. Daly, H. Eichelberger, G. Laky, and the CAA team for the valuable suggestions/comments and supporting the data analysis. This research was partly supported by the Austrian Science Fund FWF I429-N16 and I23862-N16. K.-H. Fornaçon and K.-H. Glassmeier were financially supported through grants 50OC1102 and 50OC1001 by the German Bundesministerium für Wirtschaft und Technologie and the Deutsches Zentrum für Luft- und Raumfahrt.

Edited by: H. Laakso

References

- Acuña, M. H.: Space-based magnetometers, *Rev. Sci. Instrum.*, 73, 3717–3736, doi:10.1063/1.1510570, 2002.
- Auster, H. U., Fornaçon, K. H., Georgescu, E., Glassmeier, K. H., and Motschmann, U.: Calibration of flux-gate magnetometers using relative motion, *Meas. Sci. Technol.*, 13, 1124–1131, doi:10.1088/0957-0233/13/7/321, 2002.
- Auster, H. U., Glassmeier, K. H., Magnes, W., Aydogar, O., Baumjohann, W., Constantinescu, D., Fischer, D., Fornaçon, K. H., Georgescu, E., Harvey, P., Hillenmaier, O., Kroth, R., Ludlam, M., Narita, Y., Nakamura, R., Okrafka, K., Plaschke, F., Richter, I., Schwarzl, H., Stoll, B., Valavanoglou, A., and Wiedemann, M.: The THEMIS Fluxgate Magnetometer, *Space Sci. Rev.*, 141, 235–264, doi:10.1007/s11214-008-9365-9, 2008.
- Balogh, A.: Planetary magnetic field measurements: Missions and instrumentation, *Space Sci. Rev.*, 152, 23–97, doi:10.1007/s11214-010-9643-1, 2010.
- Balogh, A., Carr, C. M., Acuña, M. H., Dunlop, M. W., Beek, T. J., Brown, P., Fornaçon, K.-H., Georgescu, E., Glassmeier, K.-H., Harris, J., Musmann, G., Oddy, T., and Schwingenschuh, K.: The Cluster Magnetic Field Investigation: overview of in-flight performance and initial results, *Ann. Geophys.*, 19, 1207–1217, doi:10.5194/angeo-19-1207-2001, 2001.
- Dougherty, M. K., Kellock, S., Southwood, D. J., Balogh, A., Smith, E. J., Tsurutani, B. T., Gerlach, B., Glassmeier, K.-H., Gliem, F., Russell, C. T., Erdos, G., Neubauer, F. M., and Cowley, S. W. H.: The Cassini magnetic field investigation, *Space Sci. Rev.*, 114, 331–383, doi:10.1007/s11214-004-1432-2, 2004.
- Fornaçon, K.-H., Georgescu, E., Kempen, R., and Constantinescu, D.: Fluxgate magnetometer data processing for Cluster, *Tech. Rep.*, Institut für Geophysik und extraterrestrische Physik, Technischen Universität Braunschweig, 38106 Braunschweig, Germany, 2011.
- Georgescu, E., Vaith, H., Fornaçon, K.-H., Auster, U., Balogh, A., Carr, C., Chutter, M., Dunlop, M., Foerster, M., Glassmeier, K.-H., Gloag, J., Paschmann, G., Quinn, J., and Torbert, R.: Use of EDI time-of-flight data for FGM calibration check on

- CLUSTER, in: Cluster and Double Star Symposium, Vol. 598 of ESA Special Publication, ESTEC, Noordwijk, the Netherlands, 2006.
- Georgescu, E., Puhl-Quinn, P., and Vaith, H. and Matsui, H.: Cross Calibration Report of the EDI Measurements in the Cluster Active Archive (CAA), http://caa.estec.esa.int/documents/CR/CAA_EST_CR_EDI_v14.pdf (last access: 29 July 2013), 2012.
- Glassmeier, K.-H., Richter, I., Diedrich, A., Musmann, G., Auster, U., Motschmann, U., Balogh, A., Carr, C., Cupido, E., Coates, A., Rother, M., Schwingschuh, K., Szegö, K., and Tsurutani, B.: RPC-MAG The Fluxgate Magnetometer in the ROSETTA Plasma Consortium, *Space Sci. Rev.*, 128, 649–670, doi:10.1007/s11214-006-9114-x, 2007.
- Glog, J. M., Carr, C., Forte, B., and Lucek, E. A.: The status of Cluster FGM data submissions to the CAA, in: Cluster and Double Star Symposium, Vol. 598 of ESA Special Publication, ESTEC, Noordwijk, the Netherlands, 2006.
- Hedgecock, P. C.: A correlation technique for magnetometer zero level determination, *Space Sci. Instrum.*, 1, 83–90, 1975.
- Kepko, E. L., Khurana, K. K., Kivelson, M. G., Elphic, R. C., and Russell, C. T.: Accurate determination of magnetic field gradients from four point vector measurements. I. Use of natural constraints on vector data obtained from a single spinning spacecraft, *IEEE T. Magn.*, 32, 377–385, doi:10.1109/20.486522, 1996.
- Leinweber, H. K., Russell, C. T., Torkar, K., Zhang, T. L., and Angelopoulos, V.: An advanced approach to finding magnetometer zero levels in the interplanetary magnetic field, *Meas. Sci. Technol.*, 19, 055104, doi:10.1088/0957-0233/19/5/055104, 2008.
- Leinweber, H. K., Russell, C. T., and Torkar, K.: In-flight calibration of the spin axis offset of a fluxgate magnetometer with an electron drift instrument, *Meas. Sci. Technol.*, 23, 105003, doi:10.1088/0957-0233/23/10/105003, 2012.
- Ludlam, M., Angelopoulos, V., Taylor, E., Snare, R. C., Means, J. D., Ge, Y. S., Narvaez, P., Auster, H. U., Le Contel, O., Larson, D., and Moreau, T.: The THEMIS magnetic cleanliness program, *Space Sci. Rev.*, 141, 171–184, doi:10.1007/s11214-008-9423-3, 2008.
- Othmer, C., Richter, I., and Fornaçon, K.-H.: Fluxgate magnetometer calibration for Cluster II, Tech. Rep., Institut für Geophysik und Meteorologie, Technischen Universität Braunschweig, 38106 Braunschweig, Germany, 2000.
- Paschmann, G., Melzner, F., Frenzel, R., Vaith, H., Parigger, P., Pagel, U., Bauer, O. H., Haerendel, G., Baumjohann, W., Scopke, N., Torbert, R. B., Briggs, B., Chan, J., Lynch, K., Morey, K., Quinn, J. M., Simpson, D., Young, C., McIlwain, C. E., Fillius, W., Kerr, S. S., Mahieu, R., and Whipple, E. C.: The Electron Drift Instrument for Cluster, *Space Sci. Rev.*, 79, 233–269, doi:10.1023/A:1004917512774, 1997.
- Paschmann, G., Scopke, N., Vaith, H., Quinn, J. M., Bauer, O. H., Baumjohann, W., Fillius, W., Haerendel, G., Kerr, S. S., Kletzing, C. A., Lynch, K., McIlwain, C. E., Torbert, R. B., and Whipple, E. C.: EDI electron time-of-flight measurements on Equator-S, *Ann. Geophys.*, 17, 1513–1520, doi:10.1007/s00585-999-1513-3, 1999.
- Paschmann, G., Quinn, J. M., Torbert, R. B., Vaith, H., McIlwain, C. E., Haerendel, G., Bauer, O. H., Bauer, T., Baumjohann, W., Fillius, W., Förster, M., Frey, S., Georgescu, E., Kerr, S. S., Kletzing, C. A., Matsui, H., Puhl-Quinn, P., and Whipple, E. C.: The Electron Drift Instrument on Cluster: overview of first results, *Ann. Geophys.*, 19, 1273–1288, doi:10.5194/angeo-19-1273-2001, 2001.
- Pudney, M. A., Carr, C. M., Schwartz, S. J., and Howarth, S. I.: Automatic parameterization for magnetometer zero offset determination, *Geosci. Instrum. Method. Data Syst.*, 1, 103–109, doi:10.5194/gi-1-103-2012, 2012.
- Quinn, J. M., Paschmann, G., Scopke, N., Jordanova, V. K., Vaith, H., Bauer, O. H., Baumjohann, W., Fillius, W., Haerendel, G., Kerr, S. S., Kletzing, C. A., Lynch, K., McIlwain, C. E., Torbert, R. B., and Whipple, E. C.: EDI convection measurements at 5–6 R_E in the post-midnight region, *Ann. Geophys.*, 17, 1503–1512, doi:10.1007/s00585-999-1503-5, 1999.
- Vaith, H., Frenzel, R., Paschmann, G., and Melzner, E.: Electron Gyro Time Measurement Technique for Determining Electric and Magnetic Fields, American Geophysical Union Geophysical Monograph Series, 103, 47–52, 1998.